universe

MDPI

Article

Quasinormal Modes for Charged Lifshitz Black Holes with Scalar Hair

Xufen Zhang [1], Shan Wu [1], Rui-Hong Yue [1], De-Cheng Zou [2,*] and Ming Zhang [3,4,*]

[1] Center for Gravitation and Cosmology, College of Physical Science and Technology, Yangzhou University, Yangzhou 225009, China; yzqzxf@gmail.com (X.Z.); rhyue@yzu.edu.cn (R.-H.Y.)
[2] College of Physics and Communication Electronics, Jiangxi Normal University, Nanchang 330022, China
[3] Faculty of Science, Xihang University, Xi'an 710077, China
[4] National Joint Engineering Research Center for Special Pump System Technology, Xihang University, Xi'an 710077, China
* Correspondence: dczou@jxnu.edu.cn (D.-C.Z.); zhangming@xaau.edu.cn (M.Z.)

Abstract

In this paper, we investigate massive charged scalar perturbations in four-dimensional charged Lifshitz–AdS black holes with scalar hair within the framework of Einstein–Maxwell–Dilaton (EMD) gravity. Using the improved asymptotic iteration method (AIM), we compute the quasinormal modes (QNMs) and explore their dependence on key parameters, including the Lifshitz dynamical exponent z, the scalar field mass and charge, and the black hole charge, under various spatial curvature settings ($k = 0, \pm 1$). Our results reveal rich and sensitive behavior in both the real and imaginary parts of the QNMs. In particular, the decay rates can exhibit monotonic or non-monotonic dependence on the black hole charge, depending on the values of z, m_s, and q_s. These findings highlight the significant role of field and geometric parameters in governing the dynamical stability of Lifshitz black holes and offer insights into the perturbative properties of non-AdS holographic systems.

Keywords: charged Lifshitz–AdS black holes; Einstein–Maxwell–Dilaton gravity; quasinormal modes; charged scalar perturbations

check for updates

Academic Editor: Gonzalo J. Olmo

Received: 6 July 2025
Revised: 4 September 2025
Accepted: 11 September 2025
Published: 13 September 2025

Citation: Zhang, X.; Wu, S.; Yue, R.-H.; Zou, D.-C.; Zhang, M. Quasinormal Modes for Charged Lifshitz Black Holes with Scalar Hair. *Universe* **2025**, *11*, 317. https://doi.org/10.3390/universe11090317

Copyright: © 2025 by the authors. Licensee MDPI, Basel, Switzerland. This article is an open access article distributed under the terms and conditions of the Creative Commons Attribution (CC BY) license (https://creativecommons.org/licenses/by/4.0/).

1. Introduction

An important extension of the holographic duality beyond high-energy physics is its application to strongly coupled systems in condensed matter physics, particularly in the study of quantum critical phenomena [1]. Such systems often display an anisotropic scaling symmetry between space and time, known as Lifshitz scaling,

$$t \mapsto \lambda^z t, \quad r \mapsto \lambda^{-1} r, \quad x_i \mapsto \lambda x_i, \tag{1}$$

where the parameter $z \geq 1$ is referred to as the dynamical or critical exponent and quantifies the degree of anisotropy. This scaling symmetry is holographically realized by the so-called Lifshitz spacetime, described by the metric

$$\mathrm{d}s^2 = -(\frac{r}{l})^{2z}\mathrm{d}t^2 + \frac{l^2}{r^2}\mathrm{d}r^2 + r^2\mathrm{d}^2\vec{x}^2, \tag{2}$$

where l denotes the characteristic length scale of the geometry. Lifshitz spacetimes can be regarded as anisotropic generalizations of the anti-de Sitter (AdS) spacetime, preserving constant negative curvature while sharing many of its geometric and physical features.

The no-hair theorem [2,3] is a core principle in black hole physics, stating that the properties of a black hole are uniquely determined by three parameters: mass, charge, and angular momentum. This theorem has been widely supported within the frameworks of Einstein's theory of gravity and Maxwell's electromagnetic theory, as the external field of a black hole in these theories follows Gauss's law, indicating that conserved quantities are closely related to the black hole's characteristics. However, with the introduction of scalar fields and other physical fields [4–7], such as the Einstein–Yang–Mills SU(2) coupled system, black holes with dilaton hair, and black holes with Skyrme hair, it has been found that the existence of these fields may lead to a violation of the no-hair theorem. Notably, in cases of conformally coupled scalar fields, "hairy black holes" can emerge, which possess additional macroscopic degrees of freedom that make their external field behavior no longer conform to the no-hair theorem [8,9]. The phenomenon of spontaneous scalarization was explored in the context of neutron stars [10], revealing that effective non-minimal coupling between the scalar field and curvature can lead to nontrivial behavior of black holes, potentially resulting in changes to the total mass. This scalarization of black holes may manifest only under strong gravitational backgrounds, and it could provide new insights into the nature of black hole scalarization with the help of emergent technologies like gravitational-wave detectors (such as LISA) and black hole shadow imaging [11]. David Garfinkle et al. first proposed a series of solutions for static, spherically symmetric charged black holes in string theory. These solutions are described by the black hole's mass, charge, and the asymptotic values of the scalar field (dilaton field), with the dilaton in string theory linearly coupled to F^2 [12]. And Gary W. Gibbons et al. introduced the dilaton field to provide a unified descriptive framework for objects such as black holes and branes in higher-dimensional theories. They also revealed the sensitive dependence of the physical properties of these objects on the dilaton coupling constant [13]. In order to address the limitations of general relativity that become apparent under extreme conditions, researchers have explored modified gravitational theories such as string theory, particularly heterotic string theory, which provides higher-order corrections ranging from the Gauss–Bonnet term to non-linear electromagnetic effects [14]. Other solutions are provided in [15,16]. Subsequently, A. Herrera-Aguila and Moreira et al. [17–19] proposed new exact black hole solutions within the framework of generalized Einstein–Maxwell–Dilaton theory, arising from the breaking of spacetime isotropic scale symmetry.

A. Herrera-Aguilar et al. [17] presented generalized Einstein–Maxwell–Dilaton gravity with a non-minimal coupling $h(\phi(r))$, where the action is

$$S = \frac{1}{16\pi}\int \mathrm{d}^4x\sqrt{-g}\Big[\frac{R-2\Lambda}{2\kappa} - \frac{1}{2}\partial_\mu\phi\partial^\mu\phi - \frac{h(\phi(r))}{4}F_{\mu\nu}F^{\mu\nu}\Big], \tag{3}$$

where $g = \det(g_{\mu\nu})$ denotes the metric determinant, R is the Ricci scalar, Λ is the cosmological constant, $F_{\mu\nu} = \partial_\mu A_\nu - \partial_\nu A_\mu$ is the field strength, and $h(\phi(r))$ is a non-minimal coupling function. The corresponding equation of motion admits a Lifshitz-type solution [17]

$$\begin{aligned} ds^2 &= -\Big(\frac{r}{l}\Big)^{2z} f(r)\,dt^2 + \frac{l^2}{r^2 f(r)}\,dr^2 + \Big(\frac{r}{l}\Big)^2(dx^2+dy^2), \\ f(r) &= 1 - \frac{a}{r^{z+2}} + \frac{b}{r^{2(z+1)}}, \quad \phi(r) = \sqrt{\frac{2(z-1)}{\kappa}}\,\ln\Big(\frac{r}{p}\Big), \end{aligned} \tag{4}$$

where a and b are integration constants with dimensions of length, p is the characteristic length scale, and $z \geq 1$ ensures the reality of the scalar field. These solutions represent asymptotically Lifshitz black holes supported by both electromagnetic and scalar fields.

Gravitational-wave detection has made significant advances in astrophysics and the study of black holes, providing a reliable method for investigating black hole oscillations or mergers [20–23]. Modern detectors like LIGO and Virgo effectively capture these signals, and by analyzing the frequency and amplitude of the waveforms, one can infer the mass, spin, and merger process of black holes. This deepens our understanding of black holes and offers new avenues for testing fundamental gravitational theories. Black holes interact with surrounding matter, producing gravitational waves that manifest as brief radiation bursts and damped oscillations, known as quasinormal modes (QNMs). QNMs are crucial for describing dissipative systems and black hole physics; the real part of the complex frequency represents the oscillation frequency, and the imaginary part reflects the decay timescale. Analyzing the QNMs from astrophysical black holes helps in understanding the existence of extra dimensions in string theory [24–26] and provides evidence for echoes in the ring-down signal [27]. In addition, the QNMs help to infer the mass and angular momentum of black holes and test the no-hair theorem of general relativity [28,29]. QNMs play an important role in assessing the stability of background spacetimes and are key to identifying the existence of black holes and their dynamical stability. This paper will investigate the QNMs of charged Lifshitz black holes with scalar hair, exploring the impact of model parameters on the dynamics of perturbation waves and testing the stability of the background configuration.

The organization of this paper is as follows. In Section 2, we introduce the theoretical framework of D-dimensional Lifshitz black holes with non-minimal coupling between the scalar and Maxwell fields and discuss scalarized Lifshitz black holes for various horizon topologies ($k = 0, \pm 1$). In Section 3, we investigate massive charged scalar perturbations in the four-dimensional case. In Section 4, we use an improved asymptotic iteration method (AIM) to calculate the QNM frequencies of charged four-dimensional Lifshitz black holes. In Section 5, we analyze the numerical results of the QNMs and study the effects of factors such as the curvature, mass, and critical dynamical exponent of the black hole on the QNMs. Finally, we conclude with closing remarks in Section 6. Note that we adopt the metric signature $(-,+,+,+,\cdots)$ for higher-dimensional spacetime and $(-,+,+,+)$ for four-dimensional spacetime.

2. Charged Lifshitz Solutions in Higher-Dimensional Spacetime

In this study, we investigate higher-dimensional solutions in generalized Einstein–Maxwell–Dilaton theory. The action of our model is given by

$$S = \frac{1}{16\pi}\int \mathrm{d}^D x\sqrt{-g}\Big[\frac{R-2\Lambda}{2\kappa} - \frac{1}{2}\partial_\mu\phi\partial^\mu\phi - \frac{h(\phi(r))}{4}F_{\mu\nu}F^{\mu\nu}\Big], \tag{5}$$

where $g = \det(g_{\mu\nu})$ denotes the metric determinant, R is the Ricci scalar, Λ is the cosmological constant, $F_{\mu\nu} = \partial_\mu A_\nu - \partial_\nu A_\mu$ is the standard Maxwell field, and $h(\phi(r))$ is a non-minimal coupling function.

Varying the action (5) with respect to the metric $g_{\mu\nu}$, dilaton field ϕ, and electromagnetic potential A_μ leads to

$$G_{\mu\nu} + \Lambda g_{\mu\nu} - \kappa T_{\mu\nu} = 0; \tag{6}$$

$$\nabla^2\phi - \frac{1}{4}\frac{\mathrm{d}h}{\mathrm{d}\phi}F_{\mu\nu}F^{\mu\nu} = 0; \tag{7}$$

$$\nabla_\nu(h(\phi(r))F^{\mu\nu}) = 0, \tag{8}$$

where $G_{\mu\nu} = R_{\mu\nu} - \frac{1}{2}Rg_{\mu\nu}$ is the Einstein tensor and $T_{\mu\nu}$ is the energy-momentum tensor:

$$T_{\mu\nu} = \partial_\mu\phi\partial_\nu\phi - \frac{1}{2}g_{\mu\nu}(\partial\phi)^2 + F_{\mu\alpha}F_\nu{}^\alpha - \frac{1}{4}F_{\alpha\beta}{}^{\alpha\beta}g_{\mu\nu}. \tag{9}$$

We assume the metric of Lifshitz spacetime takes the following form:

$$\mathrm{d}s^2 = -\left(\frac{r}{l}\right)^{2z} f(r)\mathrm{d}t^2 + \frac{\mathrm{d}r^2}{\left(\frac{r}{l}\right)^2 f(r)} + r^2\sum_{k=1}^{D-2}\mathrm{d}^2\Omega_k, \tag{10}$$

where z is the dynamical critical exponent and $\mathrm{d}^2\Omega_k$ designates the line element of a $(D-2)$-dimensional hypersurface with constant curvature $(D-2)(D-3)k$. It is given by

$$\mathrm{d}^2\Omega_k = \begin{cases} \mathrm{d}\theta_1^2 + \sin^2\theta_1(\mathrm{d}\theta_2^2 + \sin^2\theta_2(+\cdots+\sin^2\theta_{D-3}\mathrm{d}^2\theta_{D-2})) & k=1; \\ \mathrm{d}\theta_1^2 + \mathrm{d}\theta_2^2 + \ldots\mathrm{d}\theta_{D-2}^2 & k=0; \\ \mathrm{d}\theta_1^2 + \sinh^2\theta_1(\mathrm{d}\theta_2^2 + \sinh^2\theta_2(+\cdots+\sinh^2\theta_{D-3}\mathrm{d}^2\theta_{D-2})) & k=-1. \end{cases} \tag{11}$$

where D represents the total dimension of the spacetime. This hypersurface metric can take different forms depending on the curvature (i.e., the topology), which can be spherical, flat, or hyperbolic in nature. Specifically, for $k=1$, the curvature is positive, corresponding to spherical geometry; for $k=0$, the curvature is zero, corresponding to flat geometry; and for $k=-1$, the curvature is negative, corresponding to hyperbolic geometry. Each value of k defines a distinct geometric structure for the angular part of the metric, which in turn influences the overall topology and physical properties of the spacetime.

Note that the fields inherit the spacetime isometries such that they are functions of the r coordinate only. The vector potential is considered to be of a purely electric form; therefore, the field ansatzes are

$$\phi = \phi(r), \quad A = A_t(r)\mathrm{d}t. \tag{12}$$

Substituting the metric ansatz (10) and Equation (12) into the Maxwell Equation (8), we have

$$\partial_r(\sqrt{-g}h(\phi(r))F^{rt}) = 0, \tag{13}$$

which leads to

$$h'(\phi(r))A_t{}'(r)\phi(r)'r + h(\phi(r))\Big[-(z+1-D)A_t{}'(r) + rA_t{}''(r)\Big] = 0. \tag{14}$$

We can also rewrite this as

$$\Big[r^{D-1-z}A_t{}'(r)h(\phi(r))\Big]' = 0. \tag{15}$$

Integrating Equation (15) gives

$$A_t{}'(r) = \frac{r^{-(D-1-z)}}{h(\phi(r))}C_0, \tag{16}$$

with C_0 representing a constant. Let $C_0 = Ql^{D-1-z}$. Then, the above equation can be written as

$$A_t{}'(r) = \frac{Q}{h(\phi(r))}\left(\frac{l}{r}\right)^{D-1-z}, \tag{17}$$

where Q is an arbitrary constant that plays the role of the electric charge.

Dealing with the tt and rr components of Einstein field Equation (6), one finds the identity

$$E^t{}_t - E^r{}_r = \frac{f(r)[(D-2)(1-z) + r^2\kappa\phi'(r)^2]}{l^2} = 0, \tag{18}$$

which leads to

$$\phi(r) = \sqrt{\frac{(D-2)(z-1)}{\kappa}}\ln(\frac{r}{p}). \tag{19}$$

Here, p is a constant with the dimension of length, and $z \geq 1$ is required to ensure the reality of the scalar field. We further consider the components of the Einstein field equations:

$$\begin{aligned} E^r{}_r + E^{\theta_1}{}_{\theta_1} &= 2\Lambda - \frac{k(D-3)^2}{r^2} + \frac{(z+D-3)(z+D-2)f(r)}{l^2} \\ &+ \frac{r(3(z+D-2)-1)f'(r)}{2l^2} + \frac{r^2 f''(r)}{2l^2} = 0. \end{aligned} \tag{20}$$

Then, we obtain the solution $f(r)$:

$$f(r) = 1 + \frac{kl^2(D-3)^2}{r^2(z+D-4)^2} - \frac{a}{r^{z+D-2}} + \frac{b}{r^{2(z+D-3)}}, \tag{21}$$

where a and b are integration constants and the parameter Λ equals

$$\Lambda = -\frac{(z+D-3)(z+D-2)}{2l^2}, \tag{22}$$

to satisfy the asymptotic condition $\lim_{r\to\infty} g = g_{Lifshitz}$.

Substituting the solution $A_t{}'(r)$ from (17) into the tt component of the equation of motion

$$\begin{aligned} E^t{}_t &= \frac{1}{2l^2}\Big(2l^2\Lambda + (D-2)rf'(r) + r^2(\frac{r}{l})^{-2z}\kappa h(\phi(r))A_t'(r)^2 \\ &+ f(r)((D-2)(D-1) + r^2\kappa\phi'(r)^2)\Big) - \frac{k(D-2)(D-3)}{2r^2} = 0, \end{aligned} \tag{23}$$

we obtain the coupling function $h(\phi(r))$:

$$\begin{aligned} h(\phi(r)) &= -\Big(Q^2 l^D r^{3-D}\kappa\Big)\Big[l^2(2\Lambda - kr^{-2}(D-2)(D-3)) \\ &+ (D-2)rf'(r) + f(r)(D-1)(D-2) + \kappa\phi'(r)^2\Big]^{-1}. \end{aligned} \tag{24}$$

From Equations (19), (21), and (22), Equation (24) becomes

$$\begin{aligned} h(\phi(r)) &= Q^2 l^D \kappa(D-4+z)\Big[br^{3-z}(D-2)(D+z-4)^2 + r^{D-3}(z-1) \\ &\times\Big((D-3)(D-2)kl^2 + D^2 + z^2 + 2D(z-3) - 6z + 8\Big)\Big]^{-1}. \end{aligned} \tag{25}$$

Considering the scalar field (19), we express r in terms of the scalar field ϕ

$$r(\phi) = pe^{\sqrt{\frac{\kappa}{(D-2)(z-1)}}\phi}. \tag{26}$$

Therefore, we can obtain the coupling function $h(\phi)$ from Equations (25) and (26):

$$
\begin{aligned}
h(\phi) &= Q^2\kappa(D+z-4)\Big[(z-1)(D^2-5D+6)kl^{2(3-D)}p^{2(D-3)}e^{2(D-z-3)\sqrt{\frac{\kappa}{(D-2)(z-1)}}\phi} \\
&+(D-2)(D+z-4)^2bl^{2(2-D)}p^{2(1-z)}e^{2(1-2z)\sqrt{\frac{\kappa}{(D-2)(z-1)}}\phi} \\
&+(z-1)((D+z)^2-6(D+z)+8)l^{4-2D}p^{2D-4}e^{2(D-z-2)\sqrt{\frac{\kappa}{(D-2)(z-1)}}\phi}\Big]^{-1}. \qquad (27)
\end{aligned}
$$

Suppose Maxwell's equations admit trivial first integrals. We integrate Equation (13), and the gauge potential $A_t(r)$ is

$$
\begin{aligned}
A_t(r) &= A_{t0}-\frac{l^{1-z-D}r^{z+D-4}}{\kappa Q(D+z-4)^2}\Big(b(D-2)(D+z-4)^2r^{-2(D+z-4)} \\
&-(D-3)(D-2)kl^2(z-1)-r^2(z-1)(D+z-4)^2\Big). \qquad (28)
\end{aligned}
$$

where A_{t0} is an integration constant.

To confirm that the geometry remains nonsingular at infinity, we examine the local curvature invariants—the Ricci scalar R, Ricci square $R_{\mu\nu}R^{\mu\nu}$, and Kretschmann scalar $R_{\mu\nu\rho\sigma}R^{\mu\nu\rho\sigma}$, which are calculated as

$$
\begin{aligned}
&\lim_{r\to\infty}R=\frac{4\Lambda^2\left(z^2+2z+3\right)}{(z+1)(z+2)}; \\
&\lim_{r\to\infty}R_{\mu\nu}R^{\mu\nu}=\frac{8\Lambda^4\left(z^4+2z^3+5z^2+4z+6\right)}{(z+1)^2(z+2)^2}; \\
&\lim_{r\to\infty}R_{\mu\nu\rho\sigma}R^{\mu\nu\rho\sigma}=\frac{16\Lambda^4\left(z^4+2z^2+3\right)}{(z+1)^2(z+2)^2}. \qquad (29)
\end{aligned}
$$

Evidently, although the scalar field does not approach a constant, all local curvature invariants approach their Lifshitz values at infinity, and the geometry is asymptotically Lifshitz in the sense of curvature invariants. The horizon is regular provided $f(r)$ has a simple zero.

From Equation (7), the scalar field equation reads

$$
\frac{r^2\left(\frac{r}{l}\right)^{-2z}h'(\phi){A_t}'(r)^2}{2l^2}+\frac{r(rf'(r)\phi'(r)+f(r)((z+D-1)\phi'(r)+r\phi''(r)))}{l^2}=0. \qquad (30)
$$

Substituting Equations (19), (21), (27), and (28) into the above equation, we find that Equation (30) is satisfied.

3. Massive Charged Scalar Field Perturbations

In this section, we focus primarily on the four-dimensional case. This choice is motivated by the physical relevance of (3+1)-dimensional spacetimes: our observable universe, where gravitational waves have been detected, is four-dimensional. This setting also allows for a cleaner analysis of quasinormal mode structures and scalar field perturbations. The solution can be derived from Equation (21):

$$
f(r)=1+\frac{kl^2}{r^2z^2}-\frac{a}{r^{z+2}}+\frac{b}{r^{2(z+1)}}, \qquad (31)
$$

Moreover, the coupling function $h(\phi)$ in four-dimensional spacetime can be obtained from Equation (27):

$$\begin{aligned} h(\phi) &= l^4Q^2z\kappa\Big[2kl^2p^2(z-1)e^{\sqrt{2}(1-z)\sqrt{\frac{\kappa}{z-1}}\phi}+2bz^2p^{2-2z}e^{\sqrt{2}(1-2z)\sqrt{\frac{\kappa}{z-1}}\phi} \\ &\quad +zp^4(z^2+z-2)e^{\sqrt{2}(2-z)\sqrt{\frac{\kappa}{z-1}}\phi}\Big]^{-1}. \end{aligned} \tag{32}$$

For $z=1$, Equation (31) reduces to the RN-AdS black hole solution, and $\phi(r)$ equals 0 from Equation (19). Moreover, the function $h(0)$ becomes $\frac{Q^2l^6\kappa}{2b}$ from Equation (32). With regard to the action (5), we can further set $h(0)=1$ to obtain the reduced action corresponding to the RN-AdS black hole solution. This implies that the parameter b equals $\frac{Q^2l^6\kappa}{2}$ from $h(0)=\frac{Q^2l^6\kappa}{2b}=1$. We set $\kappa=1$ for simplification in the following analysis.

With regard to the charged Lifshitz black hole with scalar hair (Equation (31)), the parameter b is related to the electric charge Q, scalar field parameter p, and scalar field $\phi(r)$ from Equation (32). In particular, Refs. [30–32] adopted the dilaton coupling function $h(\phi)=e^{-2\zeta\phi}$ to obtain charged Lifshitz black holes with scalar hair, and then the parameter b can be expressed in terms of p and Q from Equation (32). Actually, this phenomenon also appears in the Einstein–Maxwell–Scalar theory [33–35], where the parameter b refers to the combination of the electric charge Q and scalar field parameter Q_s for a charged scalarized black hole.

Now we investigate a massive charged scalar field perturbation on this Lifshitz black hole. The dynamical wave equation is

$$D^\nu D_\nu\psi=m_s^2\psi, \tag{33}$$

where $D^\nu=\nabla^\nu-iq_sA^\nu$ is the gauge-covariant derivative. Here, m_s is the mass of the scalar field ψ, and q_s is the test charge of the scalar field.

Now we decompose ψ into the following standard form:

$$\psi(t,r,angles)=e^{-i\omega t}R(r)Y(angles), \tag{34}$$

where ω is the frequency and $Y(angles)$ is the spherical harmonic function related to the angular coordinates. Since Y is a spherical harmonic function, it satisfies the following equation:

$$\nabla^2_{angles}Y(\theta,\phi)=-L(L+1)Y(angles), \tag{35}$$

where $L(L+1)$ is a separation constant.

In addition, the differential equation of the radial function in the four-dimensional Lifshitz-dilaton background (10) is

$$fR''+(f'+\frac{(z+3)f}{r})R'+(\frac{q_sA_t+\omega}{r^{z+1}})^2\frac{R}{f}-(m_s^2+\frac{L(L+1)}{r^2})\frac{R}{r^2}=0. \tag{36}$$

Here, the gauge potential $A_t(r)$ is given by [36]

$$A_t(r) = A_{t0}-\frac{2l^2r^zz^{-2}(z-1)-z^2\left(2br^{-z}-(z-1)r^{z+2}\right)}{\kappa Ql^{z+3}}. \tag{37}$$

Therefore, introducing a new radial function $R(r)$ as $R(r) = K(r)/r$ and using a tortoise coordinate r_* defined by $dr_*/dr = [r^{z+1}f(r)]^{-1}$, Equation (36) can be transformed into an equation resembling the Schrödinger equation:

$$\frac{d^2K(r_*)}{dr_*^2} + [(\omega + q_sA_t)^2 - V_s(r)]K(r_*) = 0, \tag{38}$$

where the potential $V_s(r)$ is given by

$$V_s(r) = (z+1)f^2r^{2z} + fr^{2z}(m_s^2 + \frac{L(L+1)}{r^2}) + ff'r^{2z+1}. \tag{39}$$

To achieve a comprehensive understanding of the system's behavior, we need to perform a numerical analysis.

4. Quasinormal Mode Frequencies

Computing the quasinormal mode (QNM) spectrum reduces to solving a nontrivial eigenvalue problem. Several numerical approaches have been developed to tackle this challenge, including highly accurate techniques such as the pseudospectral method. In this section, we employ the improved asymptotic iteration method (AIM), a powerful semi-analytical method tailored for second-order differential equations. The AIM constructs a termination condition through an iterative procedure, enabling efficient and accurate extraction of QNM frequencies, particularly in spacetimes with intricate boundary behavior.

The key idea of the improved asymptotic iteration method (AIM) is to transform the second-order linear differential equation into a recursive form and iteratively extract a quantization condition that yields the eigenvalues. Specifically, we consider a differential equation of the form

$$\chi^{''}(x) = \zeta_0(x)\chi^{'}(x) + s_0(x)\chi(x), \tag{40}$$

where $\zeta_0(x)$ and $s_0(x)$ are smooth functions of the independent variable. Through repeated differentiation, the equation generates a sequence of functions $\zeta_n(x)$ and $s_n(x)$, defined by the recurrence relations:

$$\zeta_n(x) = \zeta_{n-1}^{'}(x) + s_{n-1}(x) + \zeta_0(x)\zeta_{n-1}(x), \quad s_n(x) = s_{n-1}^{'}(x) + s_0(x)\zeta_{n-1}(x). \tag{41}$$

The method terminates when the quantization condition

$$\delta_n(x) = s_n(x)\zeta_{n-1}(x) - s_{n-1}(x)\zeta_n(x) = 0, \tag{42}$$

is satisfied at some fixed point $x = x_0$. Solving this condition yields the eigenvalues, such as the quasinormal frequencies in black hole spacetimes.

To apply the AIM framework to our problem, we first rewrite the radial equation in a more suitable form. This is achieved by introducing the new dimensionless variable $u = 1 - \frac{r_h}{r}$, which maps the domain $r \in [r_h, \infty)$ to $u \in [0, 1)$, with the black hole horizon located at $u = 0$ and the asymptotic boundary at $u = 1$.

Under this transformation $u = 1 - \frac{r_h}{r}$, the radial Equation (36) becomes

$$\frac{r_h^{z+1}f(u)}{(1-u)^{z-1}}R''(u) + \frac{r_h^{z+1}}{(1-u)^z}\left[(z+1)f(u) + (1-u)f'(u)\right]R'(u) + \frac{r_h^{1-z}l^{2z+2}}{f(u)(1-u)^{1-z}}$$
$$(q_sA_t(u) + \omega)^2R(u) - \frac{r_h^{z+1}}{(1-u)^{z+1}}\left(m_s^2 + \frac{L(L+1)}{r_h^2}(1-u)^2\right)R(u) = 0. \tag{43}$$

In order to propose an ansatz for Equation (43), we consider the behavior of the function $R(u)$ on the horizon $(u = 0)$ and boundary $(u = 1)$. At the horizon $(u = 0)$, we have $f(0) \approx uf^{'}(0)$ and $A_t(0) = 0$; thus, Equation (43) reduces to

$$R''(u) + \frac{R'(u)}{u} + \frac{R(u)}{r_h^{2z} u^2 f'^2}\omega^2 = 0. \tag{44}$$

The solution for this equation can be written as

$$R(u \to 0) \sim C_1 u^{-\xi} + C_2 u^{\xi}, \;\; \xi = \frac{i\omega}{r_h^z f'(0)}. \tag{45}$$

Here, we impose the ingoing boundary condition at the horizon $(u = 0)$ and therefore set C_2 to vanish. At infinity, where $(u = 1)$, Equation (43), can be written as

$$R^{''}(u) + \frac{(z+1)R^{'}(u)}{1-u} - \frac{m_s^2 R(u)}{(1-u)^2} = 0. \tag{46}$$

The solution to this equation can be written as

$$R(u \to 1) \sim D_1(1-u)^{\frac{1}{2}(z+2+\Pi)} + D_2(1-u)^{\frac{1}{2}(z+2-\Pi)}, \tag{47}$$

where

$$\Pi = \sqrt{(z+2)^2 + 4m_s^2}. \tag{48}$$

In order to impose the Dirichlet boundary condition $R(u \to 1) \to 0$, we can set $D_2 = 0$. Using the above solutions at the horizon and boundary, the general ansatz for Equation (43) can be written as

$$R(u) = u^{-\xi}(1-u)^{\frac{1}{2}(z+2+\Pi)}\chi(u). \tag{49}$$

Inserting Equation (49) into (43), we obtain

$$\chi^{''} = \zeta_0(u)\chi^{'} + s_0(u)\chi, \tag{50}$$

where the coefficient functions are given by

$$\zeta_0 = \frac{2i\omega}{r_h^z u f'(0)} - \frac{f'(u)}{f(u)} + \frac{\Pi+1}{1-u}. \tag{51}$$

Furthermore, s_0 is given by

$$\begin{aligned} s_0(u) \;\; = \;\; & \frac{r_h^{-2(z+1)}}{2(u-1)^2 u^2 f(u)^2 f'^2} \times \Big[-2r_h^2 u^2 f'^2 (1-u)^{2z}(q_s A_t(u) + \omega)^2 \\ + \;\; & uf(u)f'(0)r_h^z(2uf'(0)r_h^z(m_s^2 r_h^2 + L(L+1)(u-1)^2) + r_h^2(u-1)f'(u) \\ \times \;\; & (-uf'(0)r_h^z(\Pi + z + 2) + 2i(u-1)\omega) \\ + \;\; & 2r_h^2 f(u)^2(i(u-1)\omega f'(0)r_h^z(u\Pi + 1) - m_s^2 u^2 f'^2 r_h^{2z} + (u-1)^2\omega^2)\Big]. \end{aligned} \tag{52}$$

Now we employ the improved asymptotic iteration method (AIM) to numerically solve Equation (50). In the following, we set $L = 0$ and $l = p = 1$, and analyze scalar perturbations to explore the impact of different model parameters on the real and imaginary parts of the quasinormal frequencies related to Lifshitz black hole solutions.

5. Numerical Results

In this section, we report the numerical results for the QNMs of a scalar field around the Lifshitz black hole. We consider the four-dimensional Lifshitz model with three different horizon topologies ($k = 0, \pm 1$). The frequencies of the quasinormal modes are divided into real and imaginary parts, which determine the energy of the scalar perturbations and the stability of the system under dynamical perturbations.

5.1. Massless Charged Scalar Perturbation

Figures 1–3 display the trajectories of the quasinormal frequencies $\omega = \omega_R + i\omega_I$ in the complex frequency plane for a hairy Lifshitz black hole under perturbations of a charged massless scalar field. The focus is on how the variation of black hole charge $b \in (0, b_{\text{ext}})$ affects the QNMs. The fixed parameters used are as follows: black hole mass $a = 3$, scalar field mass $m_s = 0$, scalar field charge $q_s = 1$, spatial curvature parameter $k = 0, \pm 1$, and $L = 0$, denoting the fundamental mode. The five subplots correspond to different values of the Lifshitz dynamical critical exponent z, ranging from $z = 1$ to $z = 2.75$. As the black hole charge b increases (indicated by the direction of the arrows), the QNMs trace different trajectories in the complex plane, with their behavior significantly depending on the value of z.

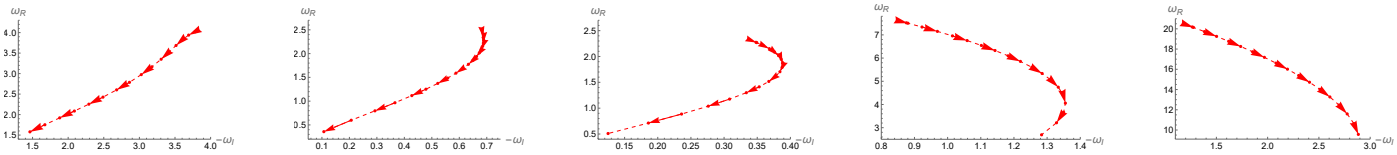

(**a**) $z = 1$ (**b**) $z = 1.65$ (**c**) $z = 1.7$ (**d**) $z = 2$ (**e**) $z = 2.75$

Figure 1. $a = 3, m_s = 0, q_s = 1, k = 0, L = 0, Q = 1$, with b ranging from 0 to near its extremal value.

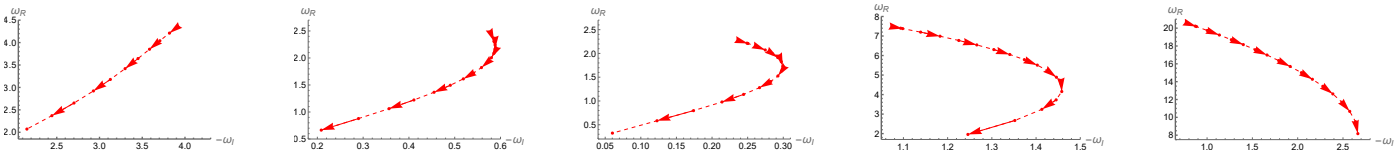

(**a**) $z = 1$ (**b**) $z = 1.7$ (**c**) $z = 1.75$ (**d**) $z = 2$ (**e**) $z = 2.8$

Figure 2. $a = 3, m_s = 0, q_s = 1, k = 1, L = 0, Q = 1$, with b ranging from 0 to near its extremal value.

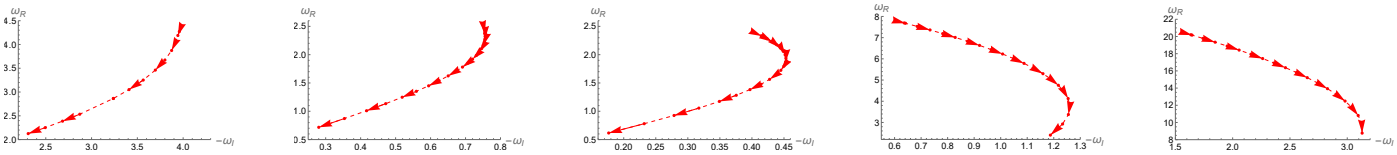

(**a**) $z = 1$ (**b**) $z = 1.6$ (**c**) $z = 1.65$ (**d**) $z = 2$ (**e**) $z = 2.7$

Figure 3. $a = 3, m_s = 0, q_s = 1, k = -1, L = 0, Q = 1$, with b ranging from 0 to near its extremal value.

When z is small (e.g., $z = 1$ and 1.7), both ω_R and $|\omega_I|$ decrease as q increases, indicating a reduction in the oscillation frequency and a slower decay rate—that is, the perturbations last longer. For intermediate values such as $z = 1.75$ and 2, $|\omega_I|$ exhibits non-monotonic behavior: it first increases and then decreases, suggesting a shift in damping characteristics at a certain threshold. When $z = 2.8$, the trend is completely reversed—$|\omega_I|$ increases monotonically with b, implying that the perturbations decay more rapidly as the black hole charge increases. These results indicate that the Lifshitz exponent z plays a crucial

role in determining the stability of the black hole, governing whether the perturbations tend to persist or dissipate quickly.

Figures 4–6 illustrate the trajectories of the quasinormal frequencies $\omega = \omega_R + i\omega_I$ in the complex frequency plane for a hairy Lifshitz black hole under perturbations from a charged massless scalar field. The focus is on the effect of the scalar field charge q_s on the behavior of the QNMs. The fixed parameters used are as follows: black hole mass $a = 3$, scalar field mass $m_s = 0$, Lifshitz dynamical critical exponent $z = 2$, spatial curvature parameter $k = 0, \pm 1$, and $L = 0$, indicating the fundamental mode. The five subfigures correspond to different values of the scalar field charge q_s. As the black hole charge b increases (indicated by the direction of the arrows), the QNMs trace distinct trajectories in the complex plane, and their behavior depends significantly on the value of q_s.

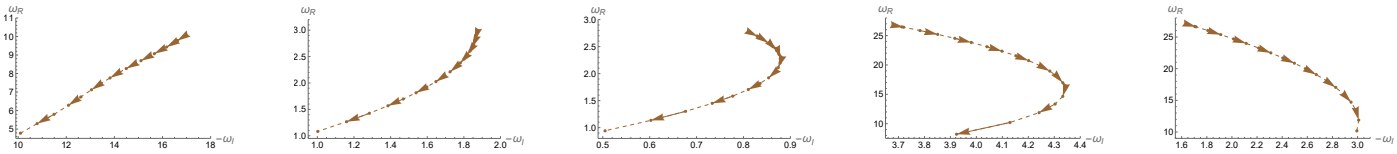

(a) $q_s = 0.01$ **(b)** $q_s = 0.6$ **(c)** $q_s = 0.7$ **(d)** $q_s = 2$ **(e)** $q_s = 2.2$

Figure 4. $a = 3, m_s = 0, k = 0, z = 2, L = 0, Q = 1$, with b ranging from 0 to near its extremal value.

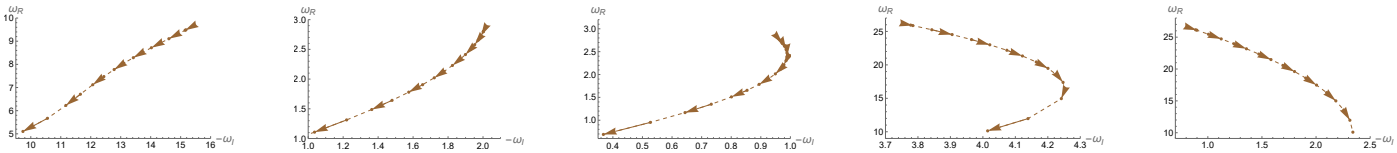

(a) $q_s = 0.01$ **(b)** $q_s = 0.6$ **(c)** $q_s = 0.7$ **(d)** $q_s = 2$ **(e)** $q_s = 2.3$

Figure 5. $a = 3, m_s = 0, k = 1, z = 2, L = 0, Q = 1$, with b ranging from 0 to near its extremal value.

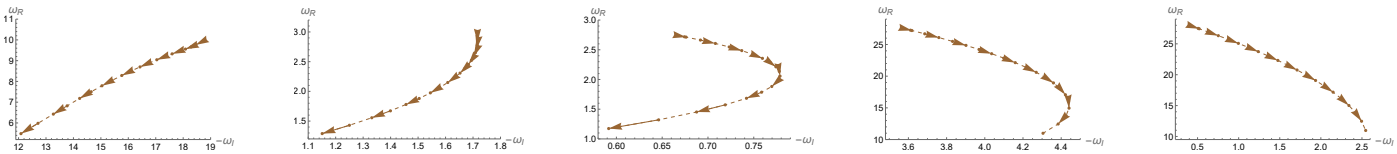

(a) $q_s = 0.01$ **(b)** $q_s = 0.6$ **(c)** $q_s = 0.7$ **(d)** $q_s = 2$ **(e)** $q_s = 2.3$

Figure 6. $a = 3, m_s = 0, k = -1, z = 2, L = 0, Q = 1$, with b ranging from 0 to near its extremal value.

When q_s is small (e.g., $q_s = 0.01$ and 0.6), both ω_R and $|\omega_I|$ decrease with increasing q, indicating a lower oscillation frequency and a slower decay rate—in other words, the perturbations persist for a longer duration. At intermediate values such as $q_s = 0.7$ and 2, $|\omega_I|$ exhibits non-monotonic behavior: it first increases and then decreases, suggesting a transition in the damping characteristics at a certain threshold. When $q_s = 2.2$, the trend is fully reversed, and $|\omega_I|$ increases monotonically with b, implying that the perturbations decay faster as the black hole charge increases. These results demonstrate that the scalar field charge q_s has a significant influence on the stability of the black hole, determining whether the perturbations tend to persist or dissipate rapidly.

5.2. Massive Charged Scalar Perturbations

Here we display only the quasinormal modes for massive scalar perturbations with $k = 0$, while the results for $k = \pm 1$ are included in Appendix A for reference.

Figure 7 displays the trajectories of the quasinormal frequencies $\omega = \omega_R + i\omega_I$ in the complex frequency plane for massive charged scalar perturbations in the background of charged Lifshitz black holes with scalar hair. We examine the impact of varying the black

hole charge b from 0 to near its extremal value on the QNMs. The fixed parameters are as follows: black hole mass $a = 3$, scalar field mass $m_s = 1$, scalar field charge $q_s = 1$, curvature parameter $k = 0$, and $L = 0$, indicating the fundamental mode. The five subfigures correspond to different values of the Lifshitz dynamical critical exponent z, ranging from $z = 1$ to $z = 2.75$. As the black hole charge b increases (indicated by the direction of the arrows), the QNMs trace different trajectories in the complex plane, and their behavior is significantly influenced by the value of z.

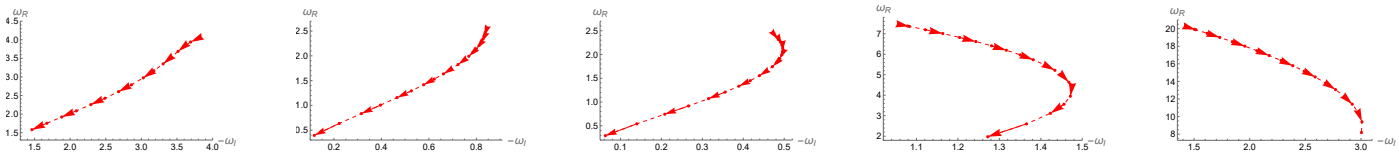

(**a**) $z = 1$ (**b**) $z = 1.65$ (**c**) $z = 1.7$ (**d**) $z = 2$ (**e**) $z = 2.75$

Figure 7. $a = 3, m_s = 1, q_s = 1, k = 0, L = 0, Q = 1$, with b ranging from 0 to near its extremal value.

For smaller values of z (e.g., $z = 1$ and 1.7), both ω_R and $|\omega_I|$ decrease as q increases, indicating that the oscillation frequency of the perturbation decreases and the decay slows, meaning the perturbation persists longer. For $z = 1.7$ and $z = 2$, $|\omega_I|$ exhibits non-monotonic behavior: it first increases and then decreases, suggesting a transition in the decay properties at a certain threshold of q. When $z = 2.75$, the trend completely reverses, and $|\omega_I|$ increases monotonically with b, implying that the perturbation decays faster as the black hole becomes more charged. These results indicate that the Lifshitz exponent z has a significant influence on the stability of the black hole, determining whether the perturbation tends to persist for a long time or decay rapidly.

Figure 8 shows the trajectories of quasinormal frequencies $\omega = \omega_R + i\omega_I$ in the complex frequency plane for a hairy Lifshitz black hole under perturbations of a massive charged scalar field. The main focus is on how the scalar field charge q_s affects the behavior of the QNMs. The fixed parameters used are: black hole mass $a = 3$, scalar field mass $m_s = 1$, Lifshitz dynamical critical exponent $z = 2$, spatial curvature parameter $k = 0$, and $L = 0$, denoting the fundamental mode. The five subplots correspond to different values of the scalar field charge q_s. As the black hole charge b increases (indicated by the direction of the arrows), the QNMs trace different paths in the complex plane, with their behavior strongly depending on the value of q_s.

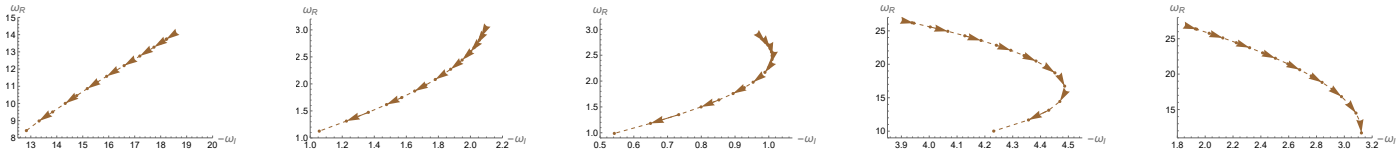

(**a**) $q_s = 0.01$ (**b**) $q_s = 0.6$ (**c**) $q_s = 0.7$ (**d**) $q_s = 2$ (**e**) $q_s = 2.2$

Figure 8. $a = 3, m_s = 1, k = 0, z = 2, L = 0, Q = 1$, with b ranging from 0 to near its extremal value.

When q_s is small (e.g., $q_s = 0.01$ and 0.6), both ω_R and $|\omega_I|$ decrease with increasing b, indicating a lower oscillation frequency and a slower decay rate, i.e., the perturbations persist longer. For $q_s = 0.7$ and 2, $|\omega_I|$ exhibits non-monotonic behavior, first increasing and then decreasing, suggesting a transition in the damping behavior at a certain threshold. When $q_s = 2.2$, the trend is completely reversed: $|\omega_I|$ increases monotonically with b, implying that the perturbations decay faster as the black hole charge increases. These results demonstrate that the scalar field charge q_s significantly influences black hole stability, determining whether perturbations tend to linger or dissipate rapidly.

5.3. m_s-Dependence

Figure 9 illustrates the trajectories of the quasinormal frequencies $\omega = \omega_R + i\omega_I$ in the complex frequency plane for a hairy Lifshitz black hole under perturbations by a massive charged scalar field. The focus is on how the scalar field mass m_s affects the behavior of the QNMs. The fixed parameters are as follows: black hole mass $a = 3$, scalar field charge $q_s = 1$, Lifshitz dynamical critical exponent $z = 2$, and $L = 0$, representing the fundamental mode. The black hole charge is set to $Q = 1$, and the scalar perturbation parameter b ranges from 0 to values approaching its extremal value. The arrows indicate the direction of increasing b. Each subplot corresponds to a different value of the scalar field mass: $m_s = 0.01, 3, 3.5, 6$.

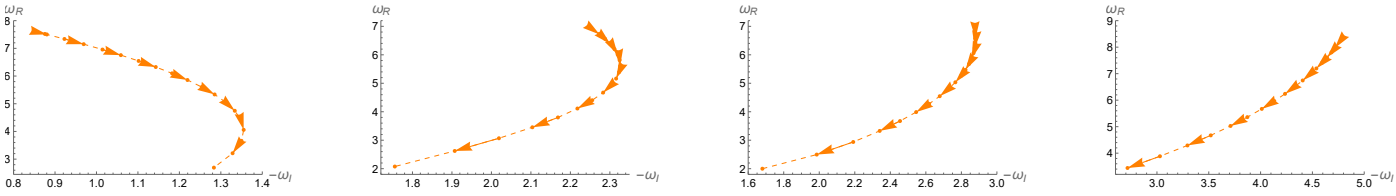

(**a**) $m_s = 0.01$ (**b**) $m_s = 3$ (**c**) $m_s = 3.8$ (**d**) $m_s = 6$

Figure 9. $a = 3, q_s = 1, k = 0, z = 2, L = 0, Q = 1$, with b ranging from 0 to near its extremal value.

For spatial curvature parameter $k = 0$, when the scalar mass m_s is small (Figure 9a), the QNM curves exhibit decreasing ω_R and $|\omega_I|$ with increasing b, indicating a lower oscillation frequency and a slower decay rate, i.e., a longer-lasting perturbation. As m_s increases, $|\omega_I|$ exhibits non-monotonic behavior—first increasing and then decreasing—suggesting a transition in the damping characteristics at a certain threshold. In contrast, when the spatial curvature is $k = 1$, non-monotonic features already appear in Figure 9a even at small m_s: as b increases, ω_R decreases monotonically, while $|\omega_I|$ first increases and then decreases, indicating a reversal in the decay rate in the intermediate b region. As m_s increases (Figure 9b–d), this non-monotonicity in $|\omega_I|$ gradually disappears. When $m_s = 6$, regardless of the value of k, $|\omega_I|$ decreases monotonically with increasing b, implying that a larger scalar mass enhances the stability of the perturbation and prolongs the decay time. Overall, the scalar field mass is a key factor in determining the behavior of perturbations and the dynamical stability of the black hole.

6. Conclusions and Discussion

In this work, we have investigated the quasinormal modes (QNMs) of charged scalar perturbations around four-dimensional Lifshitz black holes with scalar hair, focusing on the interplay between the Lifshitz exponent, scalar field parameters, and black hole charge in determining the stability and dynamical properties of the system. Both massless and massive scalar fields were considered. Their effects were systematically studied under variations in spatial curvature ($k = 0, \pm 1$) and in black hole charge b. Our findings highlight a rich landscape of dynamical behavior that depends sensitively on the values of key parameters such as the Lifshitz dynamical critical exponent z, scalar field charge q_s, and scalar field mass m_s.

For massless charged scalar fields, we found that the Lifshitz exponent z plays a decisive role in modulating the evolution of perturbations. When z is small, both the real part ω_R and the magnitude of the imaginary part $|\omega_I|$ decrease with increasing black hole charge b, indicating that the perturbations become less oscillatory and decay more slowly, thereby persisting longer. However, for moderate values of z, non-monotonic behavior in $|\omega_I|$ emerges: it first increases and then decreases with b, suggesting a critical threshold beyond which the damping mechanism reverses. At higher values like $z = 2.8$, the trend

completely reverses: $|\omega_I|$ increases monotonically with b, leading to faster decay and improved stability. These results emphasize the crucial role of the Lifshitz exponent in controlling the timescale of perturbation dissipation.

When we varied the scalar field charge q_s while keeping the field massless and fixing $z = 2$, a similar nontrivial pattern emerged. For small q_s, the system exhibits reduced oscillation and longer-lived perturbations with increasing b. As q_s increases to intermediate values, the decay rate shows a non-monotonic trend. For large charges such as $q_s = 2.2$, the perturbations decay faster with increasing black hole charge. This again signals a transition in dynamical behavior and implies that the scalar charge is a key parameter governing the system's response to perturbations.

For massive charged scalar fields, the qualitative picture remains but becomes more intricate due to the additional parameter m_s. Our analysis reveals that increasing scalar mass tends to suppress oscillations and prolong perturbation decay, especially when $k = 0$ or $k = -1$. A notable non-monotonic transition in the imaginary part of the QNMs arises for intermediate scalar masses; this transition then vanishes as m_s becomes large, suggesting enhanced damping stability in such regimes. Interestingly, in the case of positive curvature ($k = 1$), this non-monotonicity in the decay rate appears even at small m_s, highlighting the influence of spatial geometry on perturbative dynamics. When the scalar field mass is large ($m_s = 6$), the decay rate decreases monotonically with b regardless of the curvature, indicating that a sufficiently massive scalar field can enhance the black hole's resistance to dynamical perturbations.

In conclusion, our results show that the stability and decay characteristics of scalar perturbations in Lifshitz black holes with scalar hair are governed by a subtle competition among the black hole charge, Lifshitz exponent, scalar field charge, and scalar mass. The appearance of non-monotonic behavior in the damping rates underlines the possibility of critical transitions in the perturbative dynamics. This study not only provides a deeper understanding of the stability of Lifshitz black holes but also serves as a starting point for exploring more general dynamical processes in non-AdS, anisotropic geometries. Future work may extend this analysis to vector or gravitational perturbations, or explore the holographic implications of QNMs in strongly coupled field theories with Lifshitz scaling.

Author Contributions: Conceptualization, D.-C.Z. and M.Z.; methodology, D.-C.Z. and M.Z.; software, X.Z. and S.W.; validation, X.Z. and S.W.; formal analysis, X.Z. and S.W.; investigation, X.Z. and S.W.; resources, X.Z.; data curation, X.Z. and S.W.; writing—original draft preparation, X.Z.; writing—review and editing, D.-C.Z. and M.Z.; visualization, X.Z. and S.W.; supervision, R.-H.Y.; project administration, D.-C.Z. and M.Z.; funding acquisition, D.-C.Z. and M.Z. All authors have read and agreed to the published version of the manuscript.

Funding: This research was funded by Natural Science Foundation of China (NNSFC) (Grant No.12365009), the Jiangxi Provincial Natural Science Foundation (Grant No. 20232BAB201039), and the Natural Science Basic Research Program of Shaanxi (Program No.2023-JC-QN-0053).

Data Availability Statement: The original contributions presented in this study are included in the article. Further inquiries can be directed to the corresponding author.

Acknowledgments: We appreciate Sheng-Yuan Li for helpful discussion.

Conflicts of Interest: The authors declare no conflict of interest.

Appendix A. Supplementary Plots for Massive Scalar Field Perturbations

Here we include the QNM spectra for massive scalar field perturbations with $k = +1$ and $k = -1$, which were omitted from the main text for brevity. The results are qualitatively similar to those for $k = 0$ and are presented here for completeness.

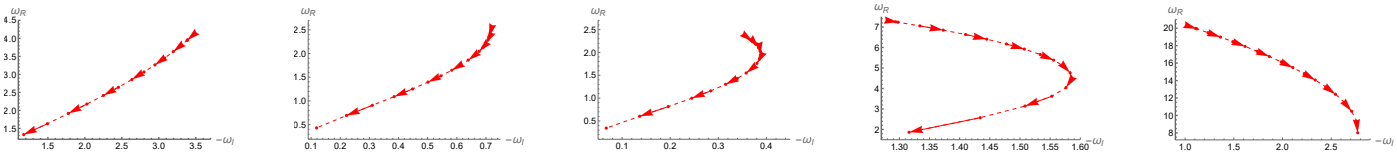

(a) $z = 1$ **(b)** $z = 1.7$ **(c)** $z = 1.75$ **(d)** $z = 2$ **(e)** $z = 2.8$

Figure A1. $a = 3, m_s = 1, q_s = 1, k = 1, L = 0, Q = 1$, with b ranging from 0 to near its extremal value.

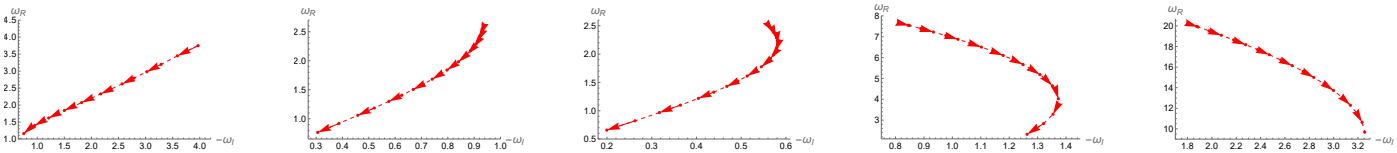

(a) $z = 1$ **(b)** $z = 1.6$ **(c)** $z = 1.65$ **(d)** $z = 2$ **(e)** $z = 2.7$

Figure A2. $a = 3, m_s = 1, q_s = 1, k = -1, L = 0, Q = 1$, with b ranging from 0 to near its extremal value.

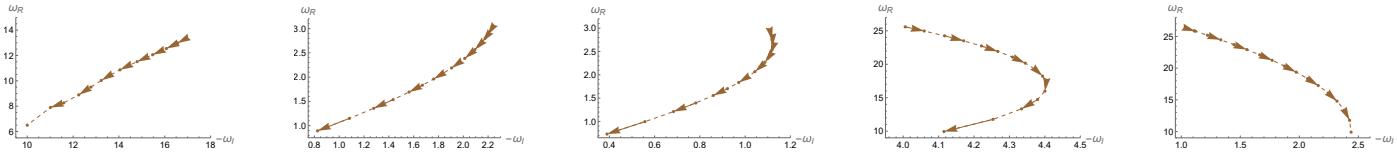

(a) $q_s = 0.01$ **(b)** $q_s = 0.6$ **(c)** $q_s = 0.7$ **(d)** $q_s = 2$ **(e)** $q_s = 2.5$

Figure A3. $a = 3, m_s = 1, k = 1, z = 2, L = 0, Q = 1$, with b ranging from 0 to near its extremal value.

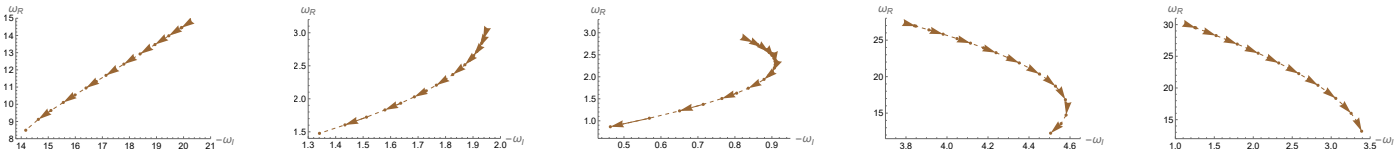

(a) $q_s = 0.01$ **(b)** $q_s = 0.6$ **(c)** $q_s = 0.7$ **(d)** $q_s = 2$ **(e)** $q_s = 2.3$

Figure A4. $a = 3, m_s = 1, k = -1, z = 2, L = 0, Q = 1$, with b ranging from 0 to near its extremal value.

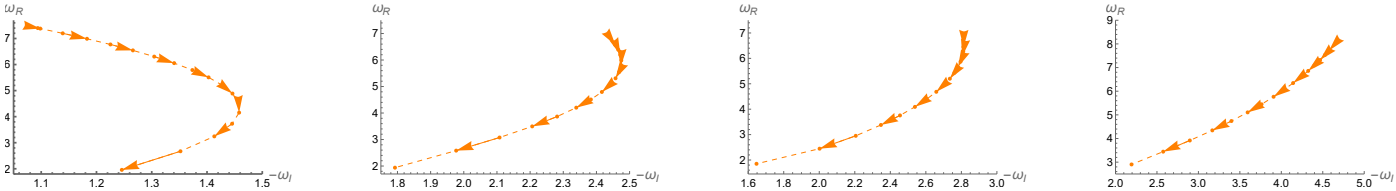

(a) $m_s = 0.01$ **(b)** $m_s = 3$ **(c)** $m_s = 3.5$ **(d)** $m_s = 6$

Figure A5. $a = 3, q_s = 1, k = 1, z = 2, L = 0, Q = 1$, with b ranging from 0 to near its extremal value.

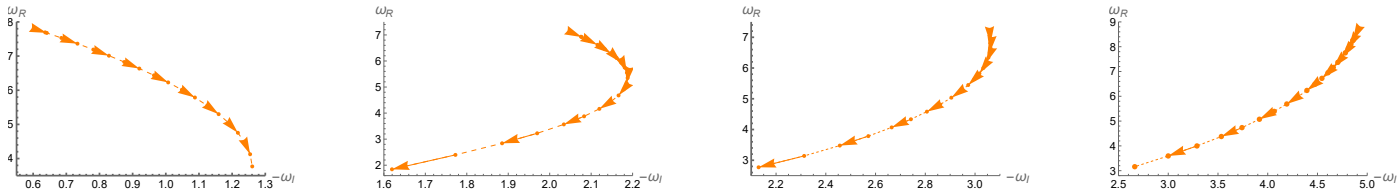

(**a**) $m_s = 0.01$ (**b**) $m_s = 3$ (**c**) $m_s = 4.2$ (**d**) $m_s = 6$

Figure A6. $a = 3, q_s = 1, k = -1, z = 2, L = 0, Q = 1$, with b ranging from 0 to near its extremal value.

References

1. Kachru, S.; Liu, X.; Mulligan, M. Gravity duals of Lifshitz-like fixed points. *Phys. Rev. D* **2008**, *78*, 106005. [CrossRef]
2. Ruffini, R.; Wheeler, J.A. Introducing the black hole. *Phys. Today* **1971**, *24*, 30. [CrossRef]
3. Bekenstein, J.D. Nonexistence of baryon number for static black holes. *Phys. Rev. D* **1972**, *5*, 1239–1246. [CrossRef]
4. Perry, M.J. Black Holes Are Colored. *Phys. Lett. B* **1977**, *71*, 234–236. [CrossRef]
5. Galtsov, D.V.; Ershov, A.A. Nonabelian Baldness of Colored Black Holes. *Phys. Lett. A* **1989**, *138*, 160–164. [CrossRef]
6. Kanti, P.; Mavromatos, N.E.; Rizos, J.; Tamvakis, K.; Winstanley, E. Dilatonic black holes in higher curvature string gravity. *Phys. Rev. D* **1996**, *54*, 5049–5058. [CrossRef]
7. Luckock, H.; Moss, I.black holes have skyrmion hair. *Phys. Lett. B* **1986**, *176*, 341–345. [CrossRef]
8. Saa, A. New no scalar hair theorem for black holes. *J. Math. Phys.* **1996**, *37*, 2346–2351. [CrossRef]
9. Mayo, A.E.; Bekenstein, J.D. No hair for spherical black holes: Charged and nonminimally coupled scalar field with selfinteraction. *Phys. Rev. D* **1996**, *54*, 5059–5069. [CrossRef]
10. Harada, T. Neutron stars in scalar tensor theories of gravity and catastrophe theory. *Phys. Rev. D* **1998**, *57*, 4802–4811. [CrossRef]
11. Damour, T.; Esposito-Farese, G. Tensor-scalar gravity and binary pulsar experiments. *Phys. Rev. D* **1996**, *54*, 1474–1491. [CrossRef]
12. Garfinkle, D.; Horowitz, G.T.; Strominger, A. Charged black holes in string theory. *Phys. Rev. D* **1991**, *43*, 3140; Erratum in *Phys. Rev. D* **1992**, *45*, 3888. [CrossRef]
13. Gibbons, G.W.; Maeda, K.i. Black Holes and Membranes in Higher Dimensional Theories with Dilaton Fields. *Nucl. Phys. B* **1988**, *298*, 741–775. [CrossRef]
14. Bakopoulos, A.; Karakasis, T.; Mavromatos, N.E.; Nakas, T.; Papantonopoulos, E. Exact black holes in string-inspired Euler-Heisenberg theory. *Phys. Rev. D* **2024**, *110*, 2. [CrossRef]
15. Gao, C.J.; Zhang, S.N. Dilaton black holes in de Sitter or Anti-de Sitter universe. *Phys. Rev. D* **2004**, *70*, 124019. [CrossRef]
16. Yu, S.; Qiu, J.; Gao, C. Constructing black holes in Einstein–Maxwell-scalar theory. *Class. Quant. Grav.* **2021**, *38*, 105006. [CrossRef]
17. Herrera-Aguilar, A.; Higuita-Borja, D.F.; Méndez-Zavaleta, J.A. Scalarization-like mechanism through spacetime anisotropic scaling symmetry. *Phys. Rev. D* **2021**, *103*, 124025. [CrossRef]
18. Moreira, D.C.; Lemos, A.S.; Brito, F.A. Charged Lifshitz black holes from general covariance breaking. *Class. Quant. Grav.* **2024**, *41*, 045004. [CrossRef]
19. Andrade, I.; Marques, M.A.; Menezes, R.; Moreira, D.C. Spatially localized scalar structures on hyperscaling violating geometries. *arXiv* **2024** , arXiv:2401.14082. [CrossRef]
20. Konoplya, R.A.; Zhidenko, A. Quasinormal modes of black holes: From astrophysics to string theory. *Rev. Mod. Phys.* **2011**, *83*, 793–836 . [CrossRef]
21. Kokkotas, K.D.; Schmidt, B.G. Quasinormal modes of stars and black holes. *Living Rev. Rel.* **1999**, *2*, 2. [CrossRef]
22. Wang, B. Perturbations around black holes. *Braz. J. Phys.* **2005**, *35*, 1029–1037. [CrossRef]
23. Berti, E.; Cardoso, V.; Gonzalez, J.A.; Sperhake, U. Mining information from binary black hole mergers: A Comparison of estimation methods for complex exponentials in noise. *Phys. Rev. D* **2007**, *75*, 124017. [CrossRef]
24. Chakraborty, S.; Chakravarti, K.; Bose, S.; SenGupta, S. Signatures of extra dimensions in gravitational waves from black hole quasinormal modes. *Phys. Rev. D* **2018**, *97*, 104053. [CrossRef]
25. Aneesh, S.; Bose, S.; Kar, S. Gravitational waves from quasinormal modes of a class of Lorentzian wormholes. *Phys. Rev. D* **2018**, *97*, 124004. [CrossRef]
26. Visinelli, L.; Bolis, N.; Vagnozzi, S. Brane-world extra dimensions in light of GW170817. *Phys. Rev. D* **2018**, *97*, 064039. [CrossRef]
27. Cardoso, V.; Pani, P. Testing the nature of dark compact objects: A status report. *Living Rev. Rel.* **2019**, *22*, 4. [CrossRef]
28. Berti, E.; Cardoso, V.; Will, C.M. On gravitational-wave spectroscopy of massive black holes with the space interferometer LISA. *Phys. Rev. D* **2006**, *73*, 064030. [CrossRef]
29. Isi, M.; Giesler, M.; Farr, W.M.; Scheel, M.A.; Teukolsky, S.A. Testing the no-hair theorem with GW150914. *Phys. Rev. Lett.* **2019**, *123*, 111102. [CrossRef]

30. Becar, R.; Gonzalez, P.A.; Vasquez, Y. Quasinormal modes of Four Dimensional Topological Nonlinear Charged Lifshitz Black Holes. *Eur. Phys. J. C* **2016**, *76*, 78. [CrossRef]
31. Zangeneh, M.K.; Wang, B.; Sheykhi, A.; Tang, Z.Y. Charged scalar quasi-normal modes for linearly charged dilaton-Lifshitz solutions. *Phys. Lett. B* **2017**, *771*, 257–263. [CrossRef]
32. Zangeneh, M.K.; Sheykhi, A.; Dehghani, M.H. Thermodynamics of topological nonlinear charged Lifshitz black holes. *Phys. Rev. D* **2015**, *92*, 024050. [CrossRef]
33. Fernandes, P.G.S.; Herdeiro, C.A.R.; Pombo, A.M.; Radu, E.; Sanchis-Gual, N. Spontaneous Scalarisation of Charged Black Holes: Coupling Dependence and Dynamical Features. *Class. Quant. Grav.* **2019**, *36*, 134002; Erratum in *Class. Quant. Grav.* **2020**, *37*, 049501. [CrossRef]
34. Myung, Y.S.; Zou, D.C. Stability of scalarized charged black holes in the Einstein–Maxwell–Scalar theory. *Eur. Phys. J. C* **2019**, *79*, 641. [CrossRef]
35. Myung, Y.S.; Zou, D.C. Quasinormal modes of scalarized black holes in the Einstein–Maxwell–Scalar theory. *Phys. Lett. B* **2019**, *790*, 400–407. [CrossRef]
36. Wu, S.; Qian, K.Q.; Yue, R.H.; Zhang, M.; Zou, D.C. Thermodynamics of charged Lifshitz black holes with scalar hair. *Mod. Phys. Lett. A* **2024**, *39*, 2450171. [CrossRef]

Disclaimer/Publisher's Note: The statements, opinions and data contained in all publications are solely those of the individual author(s) and contributor(s) and not of MDPI and/or the editor(s). MDPI and/or the editor(s) disclaim responsibility for any injury to people or property resulting from any ideas, methods, instructions or products referred to in the content.